SCIENTIFIC REPORTS

OPEN

SUBJECT AREAS:
BIOSENSORS
NANOPORES
SENSORS
SELF-ASSEMBLY

Received
11 January 2013

Accepted
27 March 2013

Published
16 April 2013

Correspondence and requests for materials should be addressed to H.T. (tianhe@ecust.edu.cn) or Y.T.L. (ytlong@ecust.edu.cn)

* These authors contributed equally to this work.

A Stimuli-Responsive Nanopore Based on a Photoresponsive Host-Guest System

Yi-Lun Ying[1]*, Junji Zhang[1]*, Fu-Na Meng[1], Chan Cao[1], Xuyang Yao[1], Itamar Willner[2], He Tian[1] & Yi-Tao Long[1]

[1]Key Laboratory for Advanced Materials & Department of Chemistry, East China University of Science and Technology, Shanghai 200237, P. R. China, [2]Institute of Chemistry and the Center for Nanoscience and Nanotechnology, The Hebrew University of Jerusalem, Jerusalem 91904, Israel.

The open-close states of the ion channels in a living system are regulated by multiple stimuli such as ligand, pH, potential and light. Functionalizing natural channels by using synthetic chemistry would provide biological nanopores with novel properties and applications. Here we use *para*-sulfonato-calix[4]arene-based host-guest supramolecular system to develop artificial gating mechanisms aiming at regulating wild-type α-HL commanded by both ligand and light stimuli. Using the gating property of α-hemolysin, we studied the host-guest interactions between *para*-sulfonato-calix[4]arene and 4, 4′-dipyridinium-azobenzene at the single-molecule level. Subsequently, we have extended the application of this gating system to the real-time study of light-induced molecular shuttle based on *para*-sulfonato-calix[4]arene and 4, 4′-dipyridinium-azobenzene at the single-molecule level. These experiments provide a more efficient method to develop a general tool to analyze the individual motions of supramolecular systems by using commercially available α-HL nanopores.

Supramolecular chemistry examines the weak and reversible non-covalent interactions which are focused on assembled molecular subunits and components[1–3]. Among all non-covalent interactions, the study of host-guest interaction is one of the most popular research fields which facilitate the understanding of the biological processes and functions. Researches of biomimetic architectures based on supramolecular host-guest interactions have been reported recently[4–6], such as protein assembly and immobilization, ion channels mimicking and bio-catalysis regulation. Sulfonato-calix[4]arene (SC_4), a member of the host family of calixarenes, is shaped as a truncated cone with hydrophilic upper and lower rims connected by a hydrophobic mid-region[7]. Strong complexes would be formed by binding SC_4 with basic amino acid lysine and arginine as guest molecules[8,9]. Previous studies showed that SC_4 could inhibit the ion channel mainly through an electrostatic interaction[10,11]. The apparent inhibition of SC_4 toward ion channels promoted us to further explore its potential application in developing biological systems.

α-Hemolysin (α-HL) transporter system is responsible for the translocation of molecules and ions from the target cells to induce an ultimate rupture of the cell membrane[12]. Seven monomers assemble into α-HL which inserts into the membrane (Fig. 1a)[13]. Realizing nature's functions of α-HL, it became an ideal nanoscale material for probing molecular transport and recognition processes, e.g., the analysis of nucleic acids and the development of DNA sequencing methods[14–18]. Various possible applications of α-HL nanopore-based biosensor have already been demonstrated, including the analysis of the structure of nucleic acids[19–23], the probing of peptide conformations[24–27], the monitoring of the interactions between biomolecules and binding targets[28–30] and the detection of small molecules[31]. Two synthetic host molecules, cyclodextrins and cucurbit[6]uril, have been studied by α-HL nanopore[32–35]. Especially, the cyclodextrins integrated α-HL nanopore attracts intensive attention due to its potential application in DNA sequencing. Since the open-close states of the ion channels in a living system are regulated by multiple stimuli such as ligand, pH, potential and light, here we use supramolecular SC_4-based host-guest interaction to develop artificial gating mechanisms aiming at regulating wild-type α-HL to command both ligand and light stimuli. Our results demonstrate that the open-close states of α-HL are being regulated by SC_4. The inhibition of ion current flow through α-HL reveals a voltage as well as an orientational dependence. In the presence of SC_4 at the *trans* side, it induces a long-term close-state of α-HL at the holding potential more negative than −70 mV, probably due to a collapse of the stem. The close-states of α-HL recover to the open-state at a more positive repulsive potential suggesting the existence of the electrostatic interactions between SC_4 and Lys^{131} (or Lys^{147}) in the stem of the pore (Fig. 1a). Enlightened by this mechanism, light-sensitive 4, 4′-dipyridinium-azobenzene (V^{2+}-Az)

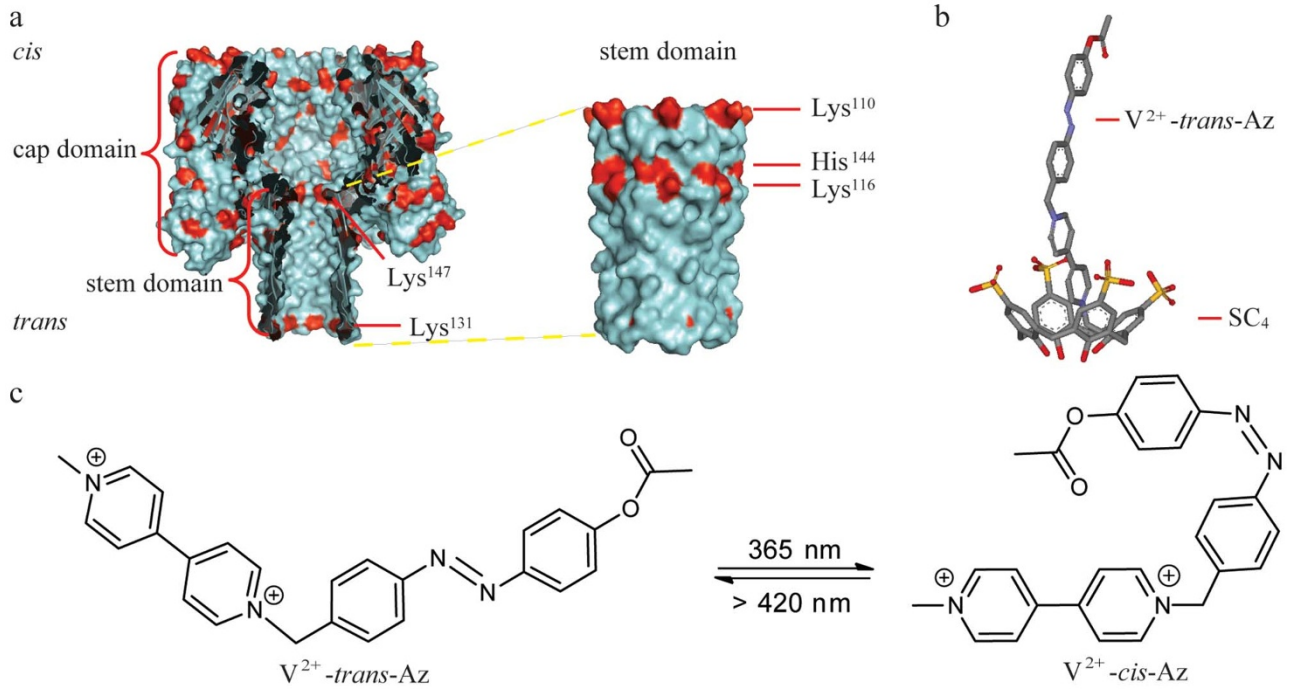

Figure 1 | Representation of an α-HL (PDB ID: 7AHL) and the interaction mechanism between SC_4 and V^{2+}-*trans*-Az. (a) An α-HL nanopore is embedded in a lipid bilayer at the Tris-EDTA (pH 8.0). The two compartments of the bilayer cell are termed *cis* and *trans*. The potential is applied through Ag/AgCl electrodes and the *cis* compartment is defined as virtual ground. Left: Cross section of α-HL which consists of a large cap domain at the exterior of the membrane and a transmembrane stem region exhibiting a diameter of 1.4 nm in its narrowest constriction. Right: the illustration of outer surface of stem domain. His, Arg and Lys as positive-charged residues are coded in red. Lys^{110}, Lys^{116}, Lys^{131}, His^{144} and Lys^{147} are positioned at the stem of α-HL, respectively. (b) The representation of SC_4:V^{2+}-*trans*-Az complex. V^{2+}-*trans*-Az is immersed into the cavity of SC_4 in its axial orientation with the viologen group being included first. (c) The photoisomeric reaction of V^{2+}-*trans*-Az to V^{2+}-*cis*-Az upon irradiation with UV light at 365 nm.

was designed as a functional guest molecule to examine the effect of host-guest interaction with SC_4 on the open-closed state regulation (Fig. 1b). Moreover, light-induced association and dissociation of the respective photoisomers of V^{2+}-Az (V^{2+}-*trans*-Az/ V^{2+}-*cis*-Az) to and from the SC_4 receptor, which would further modulate the open-close state of α-HL, were also studied by real-time probing the ion current through the pore channels (Fig. 1c). Different from previous studies[36–38], the construction of a light-regulated ion channels in our work has been achieved by non-covalent supramolecular interaction rather than the covalent modification of photoresponsive molecules inside the channel. Therefore, this would provide a more efficient approach to develop the wild-type ion channel into a general tool to analyze the individual motions of supramolecular systems.

Results

Sideness of current inhibition by SC_4. Previous studies showed that α-HL exhibited uniform and stable open-channel states at both negative and positive holding potentials[39]. The average diameter of SC_4 is about 0.2 nm which is 7 times smaller than the narrowest part of the stem region associated with α-HL[40]. The insertion of SC_4 into either the *cis* or the *trans* side of the pore is anticipated to induce the blocking of the pore, and reduce the ion current by ca. 20 % of the value of the α-HL open-channel current. Nonetheless, we find that SC_4 induces a substantially higher inhibition of the ion current and even produces a full blockage of the pore (Fig. 2). These blockages indicate that the negatively charged SC_4 stimulates a gating event on the α-HL that is amplified as anticipated from steric consideration only.

The inhibition of ion current flowing through α-HL reveals an orientational dependence (Fig. 2). The addition of SC_4 to the *trans* compartment induced both irreversible and long time reversible close-states of α-HL at holding potentials that are more negative than −70 mV (Fig. 2a–b). However, only the transient and reversible inhibitions were observed at positive holding potentials higher than +100 mV upon integration of SC_4 into the *cis* side of the pore (Fig. 2c–d). This behavior was retained even at an extreme holding potential of +140 mV and the high concentration of SC_4 ([SC_4] = 800.0 μM) as illustrated in Supplementary Fig. S1. The inter-event time-intervals of α-HL (τ_{on}) upon the *trans* side inhibitions are 16 ~ 60 times shorter than those for the *cis* side inhibitions (Fig. 3 a–b, Supplementary Fig. S1–2 and Table S1–S2), indicating that SC_4 is easier integrated with α-HL from the *trans* side. The small volume of the stem increases the interaction probability between SC_4 and the binding residues of α-HL. These results demonstrate that the interactions of SC_4 with α-HL are controlled by the steric sideness. SC_4 irreversibly binds to amino acid residues at the *trans* side of the α-HL, while it reveals reversible binding affinities upon interaction with the *cis* side of α-HL. In all the *cis* side inhibitions induced by SC_4, a Gaussian peak at the duration time (τ_{off}) of 0.36 ms was observed and its position did not change significantly under various experimental conditions (Supplementary Fig. S1 and Table S1). As described in previous studies[14,41], the durations for the translocations of polynucleotide which carries negative charges decrease with the applied potential. Since the independence of the durations (τ_{off}) for both applied potentials and concentrations of SC_4 in the *cis* side inhibitions, we ascribe the *cis* side inhibitions to the bumping rather than the translations of SC_4, e.g., a SC_4 interacts with the *cis* side of α-HL and then "bounces" off.

The inhibitions of α-HL by SC_4 from the *trans* side. We notice that the *trans*-inhibitions of α-HL exhibit strong voltage dependence. No blockages were observed at the holding potential more positive than −70 mV (Fig. 2b). The distributions of τ_{on} could be fitted by single-exponential distributions (Supplementary Fig. S2). The values of τ_{on} are inversely proportional to the applied holding potential from −70 mV to −140 mV (Fig. 3a), indicating that the probability to

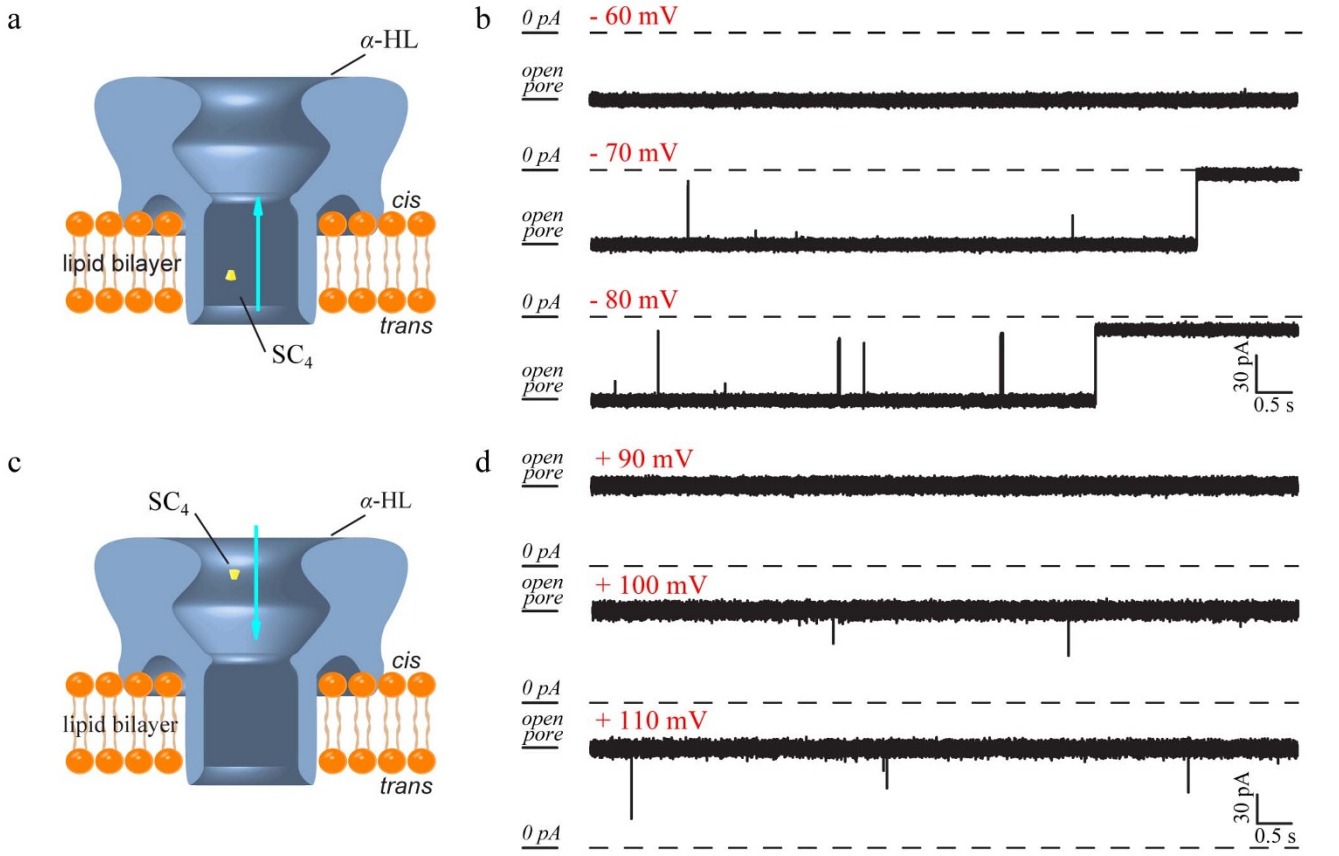

Figure 2 | Models and current traces show the 8.0 μM SC_4 binding with *α*-HL. (a) SC_4 were driven into the *trans* side of α-HL and induced the close-states of α-HL by binding with the positive-charged residues inside the stem. (b) The obtained raw data by the addition of SC_4 to the *trans* chamber at the holding potential of −60 mV (top), −70 mV (middle) and −80 mV (bottom). (c) The illustration of the inhibition of an α-HL in the presence of SC_4 at the *cis* chamber. (d) The raw data for the current traces recorded after SC_4 was driven into the *cis* side of an α-HL at the holding potential of +90 mV (top), +100 mV (middle) and +110 mV (bottom).

sustain the full open-state of α-HL is substantially lower with a more negative holding potential. This is attributed to the four negatively charged sulfonate groups associated with SC_4 which facilitate its penetration into the channel of α-HL at a more negative potential.

As the holding potential turns negative (<−70 mV), the currents for the close-states can be divided into three populations, labeled as PI, PII and PIII in Fig. 3c and Supplementary Fig. S3. For example, at the holding potential of −100 mV, the peak currents for the three populations are located at $i_I/i_0 = 0.3$, $i_{II}/i_0 = 0.65$ and $i_{III}/i_0 = 0.85$, respectively. As show in Supplementary Fig. S3–5 and Table S2, the current blockages in the population PI exhibit a substantially shorter duration time interval as compared to blockages in PII and PIII, indicating a lower association constant for the SC_4-induced inhibitions of PI. The ratios of PI type events from the total events decreased significantly from 58% to 23% throughout the increased concentration of SC_4 from 0.8 μM to 8.0 μM at the applied potential of −100 mV (Fig. 3c and Supplementary Fig. S6), revealing that lower concentration of SC_4 favors the short inhibitions. After analyzing the events in PI for the three different concentrations of SC_4 (0.8,4.0 and 8.0 μM), we found that the fitted durations in PI ($\tau_{off\text{-}PI}$) were around 0.30 ms. The value of $\tau_{off\text{-}PI}$ did not change significantly with the concentration of SC_4, even with the applied potential. Moreover, the values of $\tau_{off\text{-}PI}$ are similar to the durations for *cis* side inhibitions, confirming that the bumping events of SC_4 might account for the assignment of PI. The affinity of SC_4 is much lower to the neutral and acidic amino acids as compared to the basic amino acids[42]. The weak interactions between SC_4 and neutral and acidic amino acids may contribute to the bumping events.

The higher populations (PII and PIII) for the current inhibitions may be attributed to the two different close-states of α-HL at pH 8.0. The plot of i_{II}/i_0 and i_{III}/i_0 represent linear relationship versus potential, the slopes of which show that neither the current of partial (PII) nor complete (PIII) close-states of α-HL change significantly throughout the voltage range from −70 mV to −140 mV (Fig. 3d). The probability of the reversible inhibitions related to PI altered from 55 % to 4 % as the negative holding potential increased from −70 mV to −140 mV at $[SC_4] = 8$ μM, whereas that of PII and PIII populations increased upon applying the negative potential (Supplementary Fig. S3). The voltage-dependent distributions of the blocking currents strongly support the suggestion that the positive-charged residues are involved in the inhibitions of α-HL by SC_4. The positively charged residues inside the stem of α-HL may be distorted toward the stem end at a more negative potential[43], which poises the equilibrium process outlined in equation (1) in favor of α-HL: SC_4 and thereby increasing the probability of PII and PIII. As expected from equation (1), the value of τ_{on} decreased from 8.14 ± 0.75 s to 0.49 ± 0.24 s as the concentration of SC_4 increased from 0.8 μM to 8.0 μM (Supplementary Table S2, Fig. S7). The ratios of the number of events in PII (N_{PII}) to that of PIII (N_{PII}) show that the high potential favors the partial blocking of the pore (Supplementary Fig. S8). These results indicate that the free energies related to the partial and complete inhibition of α-HL are voltage dependent. The above results together imply that two mechanisms are operative in the pore inhibition by SC_4: i) the close-states of the α-HL are prone to occur at the enhanced negative holding potential in the presence of SC_4 at the *trans* compartment; ii) the positively charged binding sites are associated with SC_4 in the channel closures.

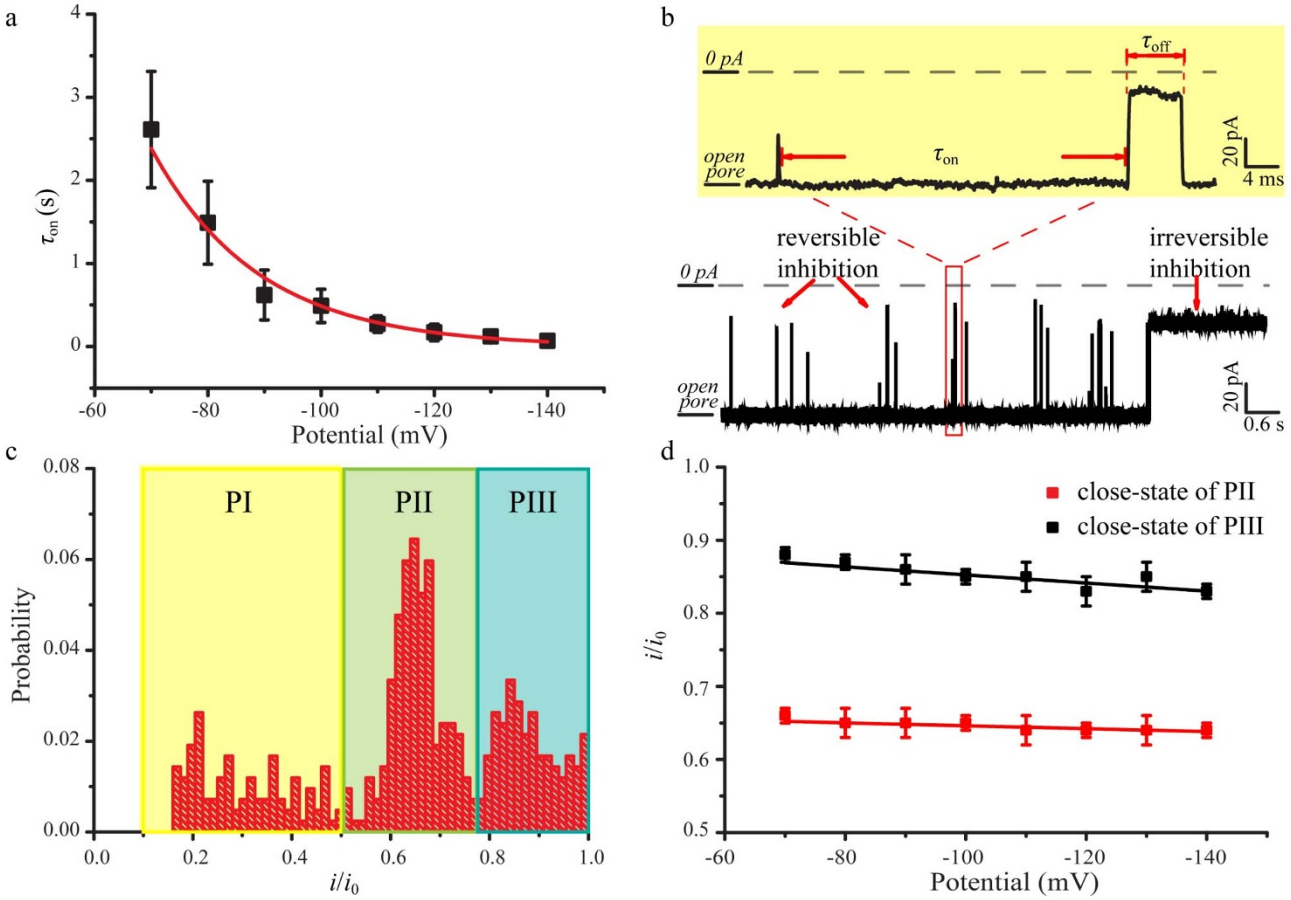

Figure 3 | 8.0 μM SC_4 induced closures of *α*-HL by the application of a negative potential at the *trans* compartment. (a) The effect of voltage on the value of τ_{on}. A single-exponential change in the value of τ_{on} was observed for the potential changing at intervals of 10 mV. The values of τ_{on} carried out by the single-exponential fittings (Supplementary Fig. S2). A large value of τ_{on} suggests that the inhibitions occur at a low frequency and vice versa. (b) The representative current trace was recorded at −100 mV. The inhibitions could be divided into reversible and irreversible blockages. The inter-inhibition interval is labeled as τ_{on}. Duration time for the reversible inhibitions defines as τ_{off}. Rectangle box illustrates the reversible blockages using higher-time resolution. (c) Current histogram at −100 mV. The peak currents for PI, PII and PIII are located at $i_I/i_0 = 0.3$, $i_{II}/i_0 = 0.65$ and $i_{III}/i_0 = 0.85$, which correspond to the blocked channel levels, respectively. (d) The linear fits for the close-state of PII and PIII versus applied potential. Red: close-state of PII; Black: close-state of PIII. The values of i_{II}/i_0 and i_{III}/i_0 were obtained by the Gaussian functions. The fitted slops for the close-state of PII and PIII are 2.0×10^{-4} V^{-1} and 5.5×10^{-4} V^{-1}, respectively.

$$\alpha\text{-HL} + SC_4 \rightleftharpoons \alpha\text{-HL} : SC_4 \quad (1)$$

In previous study, three different binding sites have been shown in the crystal structure of cytochrome-SC_4 complex[44]. Each binding site involves one lysine side chain trapped inside the cavity of SC_4, which is mainly through electrostatic interactions. As illustrated in Fig. 1a, the red colour dots depict the positive-charged amino acids and they might act as the potential electrostatic binding sites for SC_4. Lys^{110}, Lys^{116} and His^{144} are located at the outer surface of the stem domain which faces to the bilayer. Lys^{131} and Lys^{147} are positioned at the inner surface which forms the interior of the stem[13]. Due to the hydrophilicity of SC_4, its permeation into the hydrophobic bilayer is prohibited. In addition, the phospholipid head groups of bilayer would prevent the entrance of SC_4 which carries sulfonate groups at the upper-rim. Therefore, Lys^{110}, Lys^{116} and His^{144} are not likely to provide the binding sites for SC_4. In contrast, the other two lysine residues at the stem of α-HL, Lys^{131} and Lys^{147}, facing to the interior of the *β*-barrel, are probably involved in the inhibition processes by interacting with SC_4. Lys^{131}, located in the stem base (Fig. 1a) which forms a collar of charged and polar residues (Asp^{127} to Lys^{131}), is a crucial component for stabilizing the *β*-barrel of α-HL at the glycine-rich stem base[13]. Previous studies indicated that di- and trivalent cations partially affect, or reduce completely, the conductance through α-HL[45]. This channel blocking may originate from ion binding to Asp^{127} and Asp^{128} at the stem base, resulting in the collapse of the hydrophobic stem barrel[45]. Similarly, SC_4 might form a complex with the collar of Lys^{131} through electrostatic interactions, leading to the elimination of ion-pair interactions in the stem base. The crystal study demonstrated SC_4 could encapsulate L-lysine at the binding ratio of 1 : 1[46]. Subsequently, the glycine-rich stem could undergo conformational changes leading to the partial, or complete, blocking of the pore (PII/PIII in Fig. 3c). Lys^{147}, another highly potential binding site for SC_4, is the vital residue for the assembly of α-HL. The SC_4 induced inhibitions may involve the conformational changes of the stem top by binding to Lys^{147}. Alternatively, the ion pairs between Lys^{147} and Glu^{111} would be disrupted upon the binding of SC_4 to Lys^{147}, resulting in the enlargement of the pore neck by rearranging of Lys^{147} and Glu^{111} [13]. Our experiments show that the open pore current slightly increases with the probing time (Supplementary Fig. S9), suggesting that the pore neck is, indeed, enlarged. Apart from these, the hydrophobic effects[44] and the cation-π interactions[44] may also contribute to the interactions between α-HL and SC_4, leading to the conformational changes of *β*-barrel of α-HL.

By further exploring the irreversible inhibitions, we find that the open-close states of SC_4 integrated α-HL could be modulated by the holding potential. As shown in Fig. 4a and Supplementary Video,

SC_4 is repelled from the binding site by treating a repulsive potential across the bilayer. The repulsive potential is more positive than the holding potential for each irreversible inhibition. After measuring every individual irreversible inhibition, we find that −40 mV is the minimum repulsive potential which could shift the equation (1) toward the direction of dissociation (Fig. 4a). SC_4 would undergo a time-dependent repulsion process labeled as repulsion-time in Fig. 4a, prior to the dissociation of the complex at its specific value of repulsive potential. The repulsive potential will impede the access of cations into the channel and reduce the fraction of positive binding sites, resulting in the inhibitory action of the SC_4[11]. Compared the inhibitions in PIV with the ones in PV, we noted that the close-states with the larger inhibition currents exhibit more positive repulsive potentials and larger values of repulsion-time (Fig. 4b and Supplementary Fig. S10). These results might be attributed to the tight binding with SC_4 which affects the complete closure of α-HL. Thus, the collective results provide convincible evidence that the close-states of α-HL are mainly induced by strong host-guest interactions between the positive residues (probably Lys^{131} and Lys^{147}) and SC_4.

Recognition of host-guest interactions through an α-HL. The next set of experiments demonstrates that the close-state of α-HL can be modulated by ligands which induce host-guest competition inside the channel. The experiment was carried out by driving the complex of SC_4:V^{2+}-*trans*-Az into the α-HL from the *trans* side. The V^{2+}-*trans*-Az carrying two cations binds to the cavity of SC_4 in its axial orientation which was confirmed by ^{1}H NMR (Fig. 1b and Supplementary Fig. S11). The host-guest complex of SC_4:V^{2+}-*trans*-Az was formed by incubating equimolar ratios of SC_4 with V^{2+}-*trans*-Az before injected into the *trans* chamber.

In the presence of the SC_4:V^{2+}-*trans*-Az, the blockages of α-HL were rarely detected at the holding potential ranging from −70 to −130 mV. When the holding potential was negatively shifted to −140 mV, the close-states of α-HL including reversible and irreversible inhibitions were clearly generated (Fig. 5a top). As shown in Fig. 5b, the frequency for the inhibitions decreased substantially upon incubating SC_4 with V^{2+}-*trans*-Az. The value of τ_{on} for the complex is 2.41 ± 0.14 ms, which is significantly larger than that for SC_4 at −140 mV (0.09 ± 0.04 ms). These results suggest that V^{2+}-*trans*-Az, as a competitive guest molecule, hampers the host-guest interaction of SC_4 with α-HL. In order to examine the integrity of the system and the existence of open channels of α-HL, 1.6 μM SC_4 was subsequently added into the *trans* compartment which contained the complex of SC_4:V^{2+}-*trans*-Az (Fig. 5a bottom). At the holding potential of −140 mV, the value of τ_{on} decreased to 0.86 ± 0.11 ms upon the injection of added SC_4 (Fig. 5b), indicating that the pore of α-HL still exists in an intact open-state. Previous studies[8,47] demonstrated that the binding constant of SC_4:V^{2+}-*trans*-Az is about 10^5 M^{-1}, two orders of magnitude larger than that of SC_4:Lysine (K_a = 753 M^{-1}) at pH = 8. Therefore, V^{2+}-*trans*-Az probably hinders the interaction between SC_4 and α-HL by the competitive binding of SC_4. Further experiments on the viologen derivative with only one charge on one pyridine side (V^+) exhibits a value of τ_{on} of 0.34 ± 0.05 ms, revealing a much weakened binding and competition performances of V^+ due to its much lower binding constant with SC_4 (Supplementary Fig. S12–13)[47]. By virtue of SC_4 induced gating mechanism, the commercial available α-HL can be readily used to detect the competition between two guest molecules towards the binding with the host molecule.

Real-time monitoring a light-induced molecular machine by an α-HL: SC_4 system. The effect of photoisomerization of V^{2+}-*trans*-Az to the pore inhibition behavior was further studied by analyzing the frequency of the inhibitions as a function of measurement time. The complex of SC_4:V^{2+}-*trans*-Az was irradiated under λ = 365 nm for 30 min and then injected into the *trans* chamber at the potential of −100 mV. The whole experiment was carried out in dark and performed within 10 min after the addition of irradiated complex. The number of blockages was counted for a time-interval of one minute. In addition, the irreversible inhibitions should be repelled to increase the accuracy and repeatability of the counting. Therefore, the inhibitions lasted more than 5 s were treated with a positive potential of +100 mV for 1 s to relieve the close-state of α-HL in the assay of UV irradiation and the corresponding control experiments. Thus, the number of inhibitions per unit time (Fig. 5c) reveals a linear growth with slops of 1.21, 0.32 and 0.05 s^{-1} for the SC_4, SC_4:V^{2+}-*trans*-Az after UV irradiation and SC_4:V^{2+}-*trans*-Az, respectively. The frequency of inhibitions after irradiation is about 6.4 times higher than that for the SC_4:V^{2+}-*trans*-Az without irradiation. This difference in the inhibition frequencies is probably due to the photoisomerization of V^{2+}-*trans*-Az to V^{2+}-*cis*-Az isomer which perturbs the affinity between V^{2+}-Az guest and SC_4 host. Upon irradiation of SC_4:V^{2+}-*trans*-Az with UV light (λ = 365 nm), the azobenzene unit of V^{2+}-*trans*-Az isomerizes to the *cis* form, V^{2+}-*cis*-Az. Since the *cis*-azobenzene has a relatively higher dipole moment (μ = 4.4 debye) than that of the *trans*-azobenzene (μ ≈ 0 debye)[48], it can further interact with the viologen group at the

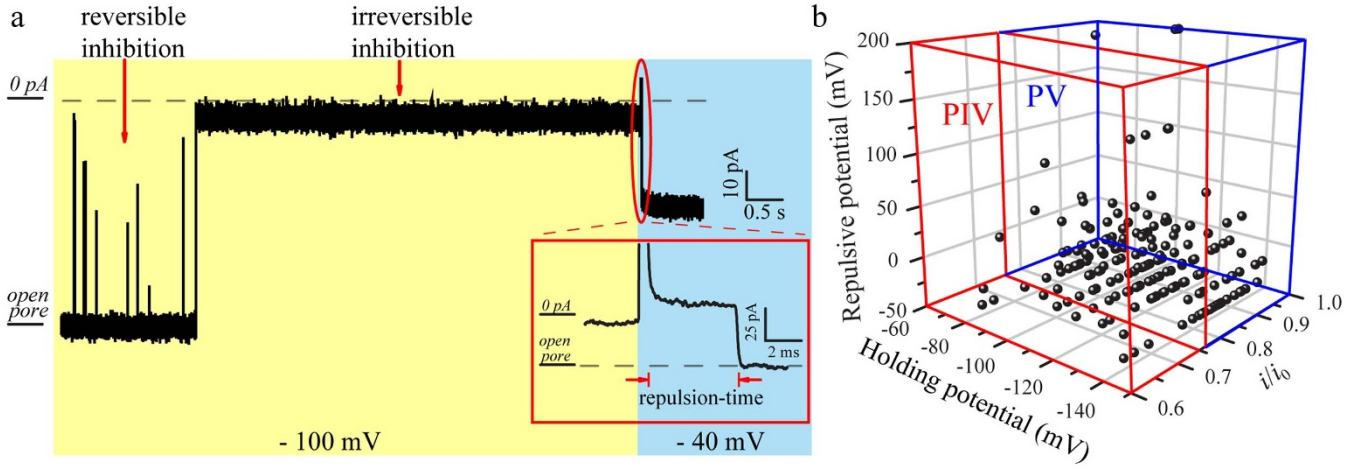

Figure 4 | Analysis of irreversible close-states of α-HL in the presence of 8.0 μM SC_4 at the *trans* compartment. (a) Representative current traces of the irreversible inhibition at the holding potential of −100 mV and the repulsive potential of −40 mV. (b) The irreversible inhibitions at the holding potential from −70 mV to −140 mV fall into two populations, PIV and PV, after treated with the repulsive potential. The majority of the irreversible inhibitions located at PV demonstrate that the irreversible close-state results from the complete closure of the channel.

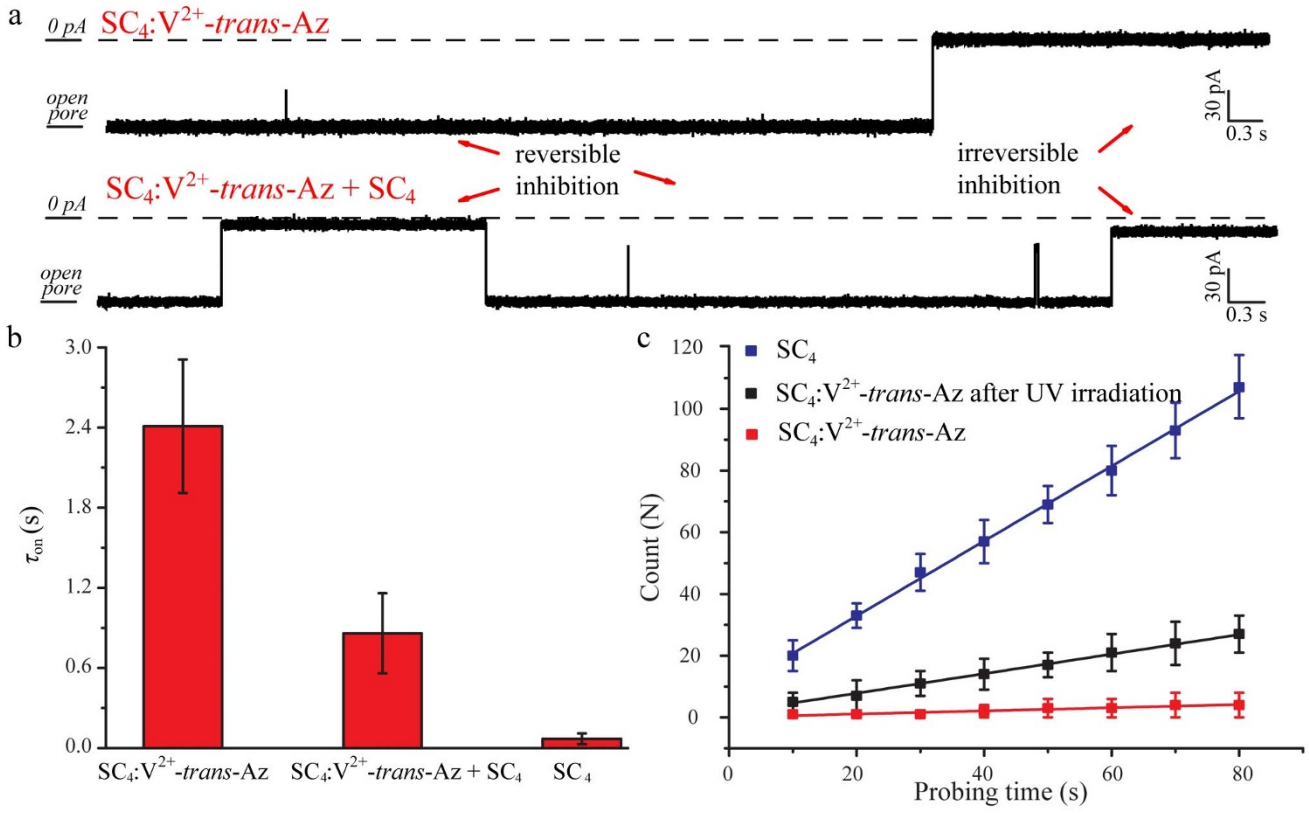

Figure 5 | Detection of host-guest interactions by an α-HL nanopore. (a) The raw data for the presence of SC_4:V^{2+}-*trans*-Az in the *trans* compartment without (top) and with (bottom) the addition of 1.6 μM SC_4 at −140 mV. (b) τ_{on} carried out in the presence of SC_4:V^{2+}-*trans*-Az, SC_4:V^{2+}-*trans*-Az with additional 1.6 μM SC_4 (SC_4:V^{2+}-*trans*-Az + SC_4) and SC_4, respectively. (c) The number of blockages versus the probing time for 8.0 μM SC_4 (blue), SC_4:V^{2+}-*trans*-Az after UV irradiation (black) and SC_4:V^{2+}-*trans*-Az (red) at the potential of −100 mV.

other end (Fig. 1c). As a result, the complexation between V^{2+}-*cis*-Az guest and SC_4 host is weakened and this would be the origin for the lower affinity of V^{2+}-*cis*-Az to SC_4. It should be noted that the inhibition frequency of SC_4:V^{2+}-*trans*-Az after irradiation is about 26% of the value in SC_4 only, according to the slop values of the inhibition number in Fig. 5c. This result is similar to the photoisomerization efficiency of *cis*-azobenzene in SC_4:V^{2+}-Az, which is about 33% calculated from ^{1}H NMR (Supplementary Fig. S14–15), revealing the efficiency of the nanopore biosensor to study the photoresponsive host-guest system at the single-molecule level.

To achieve real-time monitoring open-close state of α-HL induced by this photoresponsive host-guest system, the current traces were constantly recorded in the presence of the complex (SC_4: V^{2+}-*trans*-Az) along with irradiation under λ = 356 nm (Fig. 6a–c) at the potential of −100 mV. The structure of α-HL kept stable under

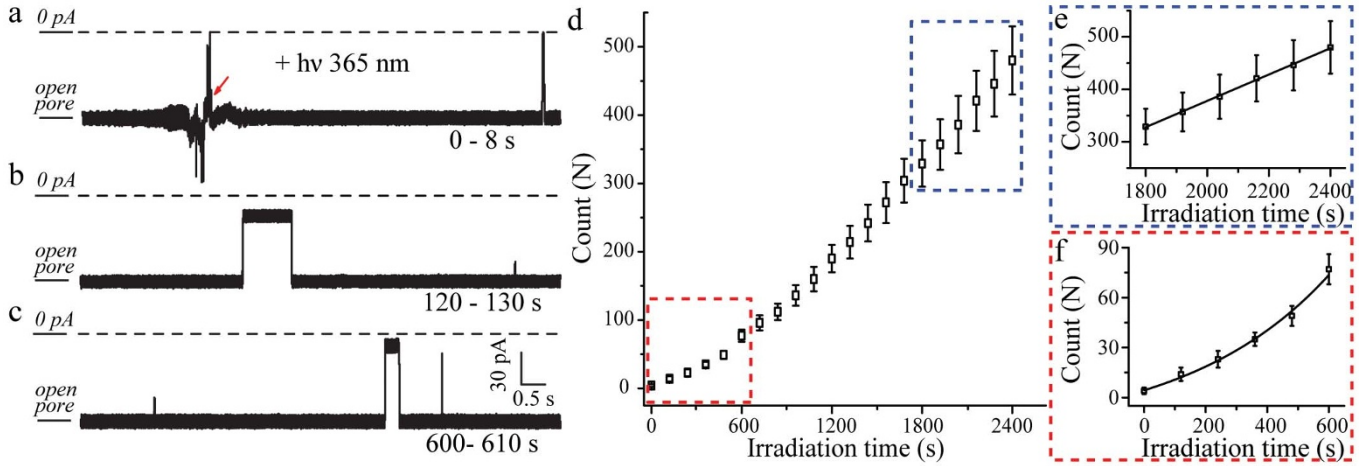

Figure 6 | Real-time monitoring the photoisomerization of SC_4:V^{2+}-Az by α-HL: SC_4 system. The current traces recorded at the irradiation time of 0–8 s (a), 120–130 s (b), 600–610 s (c) at the potential of −100 mV. (d) The number of blockages versus the UV irradiation time for the photoisomerization process. (e) The linear growth of the number of blockages yields the slop of 0.26 s^{-1} after 1800 s real-time irradiation. (f) A single-exponential function was used to fit the data obtained in the initial 10 min.

the UV irradiation in our experimental condition as shown in Supplementary Fig. S16. The number of blockages increased exponentially with the irradiation time during the initial 10 min resulting in a time constant of 316 s, and then gradually reached saturation as shown in Figure 6d–f. The traditional UV-*vis* spectroscopy studies for SC_4:V^{2+}-*trans*-Az isomerization reveal the dacay constant of 101 s (Fig. S17), confirming that the nonlinear growth is attributed to the photoisomerization of SC_4:V^{2+}-Az. After 1800 s illumination at λ = 356 nm, a linear relationship between the number of blockages and irradiation time was achieved with the saturated frequency of 0.26 s^{-1} as illustrated in Figure 6e. It should be noted that the saturated frequency obtained in real-time detection is comparable to the inhibition frequency of SC_4:V^{2+}-*trans*-Az after irradiation (0.32 s^{-1}). Therefore, this novel α-HL: SC_4 system could real-time monitor the dynamic process for the photoisomerization of SC_4:V^{2+}-Az at the single-molecule level.

Discussion

Our results demonstrate that the host compound SC_4 could efficiently induce the voltage-dependent close-states of α-HL, probably by a collapse of the stem region at high negative potentials. We suggest that Lys^{131} and Lys^{147} might be the most suitable binding sites by measuring the interactions of SC_4 with α-HL over a wide range of holding potentials. Therefore, we developed artificial gating mechanisms of α-HL triggered by the SC_4-based host-guest interactions. By virtue of this novel α-HL: SC_4 system, the functionalized α-HL has achieved to be commanded by both ligand molecule (V^{2+}-Az) and photo-stimulation at the single-molecule level for the first time. Subsequently, we have extended the application of this stimuli-responsive nanopore system to the real-time study of light-induced molecular machine based on SC_4 and V^{2+}-Az at the single-molecule level. The present study provides a general tool to probe dynamic processes of molecular machines in receptor-functionalized biomolecular nanopores, and specifically the analysis of the interactions of a light-triggered machine with the calixarene-modified α-HL nanopore was demonstrated. The various stimuli-responsive "on-off" host-guest systems could be integrated into the array of α-HL nanopores to achieve the smart logical operations at the single-molecule level.

Methods

Materials. α-HL was purchased from Sigma-Aldrich (St. Louis, MO, USA) and was used without purification. Diphytanoyl-phosphatidyl-choline was purchased from Avanti Polar Lipids Inc. (Alabaster, AL, USA). All reagents and materials are of analytical grade, and solvents were purified by standard procedures. All solutions for analytical studies were prepared with deionized water obtained by a Milli-Q System (Billerica, MA, U.S.A.).

Prior to use, the SC_4 and V^{2+}-*trans*-Az were dissolved in the buffer of Tris-EDTA (10 mM) at pH 8.0, respectively. 9.2 μL SC_4 (0.88 mM) was incubated with 10.0 μL V^{2+}-Az (0.81 mM) at the equal molar ratio before injection to the *trans* chamber. The UV irradiation of SC_4:V^{2+}-Az was carried out by a 365 nm UV hand-held lamp (UVP Inc. 115 V, 0.16 A). The UV-*vis* spectroscopy study was carried out with a PC-controlled Oceanoptics DT-Mini-2-GS situ spectrometer at a resolution of 1 nm. Unless otherwise noted, the final concentration of the analyte in the 1 mL *cis* or *trans* chamber was 8.0 μM.

Formation of the α-HL nanopore and electrical recording. As described previously[20,24,49], the lipid bilayers were created by applying 30 mg/mL diphytanoyl-phosphatidyl-choline in decane (≥99%, Sigma-Aldrich, St. Louis, MO, USA) to a 50-μm orifice in a 1-mL Delrin cup integrated into a lipid bilayer chamber (Warner Instruments, Hamden, CT, USA) with a home-made plexiglass window. Then, the chambers were filled with 1.0 M KCl and 10 mM Tris-EDTA (pH 8.0) buffer[20,24,49,50]. The chamber with a plexiglass window is assigned to *trans* chamber. The stability of the bilayer was determined by monitoring its resistance and capacitance. The two compartments of the bilayer cell are termed *cis* and *trans*, and the *cis* compartment was defined as the virtual ground. So that a positive potential indicates a higher potential in the *trans* chamber, and a positive current is the one in which cations flow from the *trans* to the *cis* side. The experiments were carried out under voltage-clamp conditions using a ChemClamp (Dagan Corporation, Minneapolis, MN, USA) instrument. The amplifier's internal low-pass Bessel filter was set at 3 kHz. Data were required at a sampling rate of 10 kHz by using a DigiData 1440A converter and a PC running PClamp 10.2 (Axon Instruments, Forest City, CA, USA). The α-HL insertion was determined by a well-defined jump in current value. Once a stable single-pore insertion was detected, the analyte was added to the *cis* or *trans* chamber, proximal to the aperture.

In the real-time assay, the UV hand-held lamp (UVP Inc. 115 V, 0.16 A) was placed 15 cm away from *trans* chamber. In order to reduce the undesirable noise, the UV hand-held lamp was wrapped by the shielding cloth. The solution in *trans* chamber was irradiated under UV-*vis* light through the plexiglass window. All of the experiments were carried out at room temperature.

Data analysis. Ionic current blockages that were larger than a threshold value of 10 pA were recorded. Data analysis was performed using home-designed software and OriginLab 8.0 (OriginLab Corporation, Northampton, MA, USA). The current blockages are described as i/i_0, where i_0 is the ionic current for the empty nanopore and i is the blockage current for the analyte partitioning into the nanopore. The values of i and i_0 were obtained by the fitted Gaussian distributions. τ_{on} (the inter-event interval) and τ_{off} (the event duration) were obtained from duration time histograms. The reported standard deviations are based on three separate experiments.

1. Champin, B., Mobian, P. & Sauvage, J.-P. Transition metal complexes as molecular machine prototypes. *Chem. Soc. Rev.* **36**, 358–366 (2007).
2. Balzani, V., Credi, A., Venturi, M. *Molecular devices and machines: concepts and perspectives for the nanoworld 2nd Edition* Wiley-VCH: Weinheim, Germany (2008).
3. Kim, K. *et al.* Functionalized cucurbiturils and their applications. *Chem. Soc. Rev.* **36**, 267–279 (2007).
4. Uhlenheuer, D. A., Petkau, K. & Brunsveld, L. Combining supramolecular chemistry with biology. *Chem. Soc. Rev.* **39**, 2817–2826 (2010).
5. Ghosh, S. & Isaacs, L. biological catalysis regulated by cucurbit [7] uril molecular containers. *J. Am. Chem. Soc.* **132**, 4445–4454 (2010).
6. Nau, W. M., Ghale, G., Hennig, A., Bakirci, H. & Bailey, D. M. Substrate-selective supramolecular tandem assays: monitoring enzyme inhibition of arginase and diamine oxidase by fluorescent dye displacement from calixarene and cucurbituril macrocycles. *J. Am. Chem. Soc.* **131**, 11558–11570 (2009).
7. Mutihac, L., Lee, J. H., Kim, J. S. & Vicens, J. Recognition of amino acids by functionalized calixarenes. *Chem. Soc. Rev.* **40**, 2777–2796 (2011).
8. Douteau-Guével, N., Coleman, A. W., Morel, J. P. & Morel-Desrosiers, N. Complexation of the basic amino acids lysine and arginine by three sulfonatocalix[n]arenes (n = 4, 6 and 8) in water: microcalorimetric determination of the Gibbs energies, enthalpies and entropies of complexation. *J. Chem. Soc., Perkin Trans* **2**, 629–634 (1999).
9. Coleman, A. *et al.* Calix[n]arenes as protein sensors. *Top. Curr. Chem.* **277**, 31–88 (2007).
10. Martos, V. *et al.* Calix[4]arene-based conical-shaped ligands for voltage-dependent potassium channels. *Proc. Nat. Acad. Sci.* **106**, 10482–10486 (2009).
11. Droogmans, G., Prenen, J., Eggermont, J., Voets, T. & Nilius, B. Voltage-dependent block of endothelial volume-regulated anion channels by calix[4]arenes. *Am. J. Physiol.- Cell Ph.* **275**, C646–C652 (1998).
12. Menestrina, G., Serra, M. D. & Lazarovici, P., eds. *Pore-forming peptides and protein toxins* (Taylor&Francis, London), Vol **5** (2005).
13. Song, L. *et al.* Structure of staphylococcal alpha-hemolysin, a heptameric transmembrane pore. *Science* **274**, 1859–1865 (1996).
14. Kasianowicz, J., Brandin, E., Branton, D. & Deamer, D. Characterization of individual polynucleotide molecules using a membrane channel. *Proc. Natl. Acad. Sci. U. S. A.* **93**, 13770–13773 (1996).
15. Branton, D. *et al.* The potential and challenges of nanopore sequencing. *Nat. Biotechnol.* **26**, 1146–1153 (2008).
16. Kumar, S. *et al.* PEG-labeled nucleotides and nanopore detection for single molecule DNA sequencing by synthesis. *Sci Rep* **2**, 684 (2012).
17. Cherf, G. M. *et al.* Automated forward and reverse ratcheting of DNA in a nanopore at 5-Å precision. *Nat. Biotechnol.* **30**, 344–348 (2012).
18. Hall, A. *et al.* Hybrid pore formation by directed insertion of α-haemolysin into solid-state nanopores. *Nat. Nanotechnol.* **5**, 874–877 (2010).
19. Wang, Y., Zheng, D., Tan, Q., Wang, M. X. & Gu, L. Q. Nanopore-based detection of circulating microRNAs in lung cancer patients. *Nat. Nanotechnol.* **6**, 668–674 (2011).
20. Ying, Y.-L., Wang, H.-Y., Sutherland, T. C. & Long, Y.-T. Monitoring of an ATP-binding aptamer and its conformational changes using an α-hemolysin nanopore. *Small* **7**, 87–94 (2011).
21. Kasianowicz, J. J., Robertson, J. W. F., Chan, E. R., Reiner, J. E. & Stanford, V. M. Nanoscopic porous sensors. *Annu. Rev. Anal. Chem.* **1**, 737–766 (2008).
22. An, N., Fleming, A. M., White, H. S. & Burrows, C. J. Crown ether–electrolyte interactions permit nanopore detection of individual DNA abasic sites in single molecules. *Proc. Natl. Acad. Sci. U. S. A.* **109**, 11504–11509 (2012).
23. Olasagasti, F. *et al.* Replication of individual DNA molecules under electronic control using a protein nanopore. *Nat. Nanotechnol.* **5**, 798–806 (2010).
24. Wang, H.-Y., Ying, Y.-L., Li, Y., Kraatz, H.-B. & Long, Y.-T. Nanopore analysis of -amyloid peptide aggregation transition induced by small molecules. *Anal. Chem.* **83**, 1746–1752 (2011).
25. Movileanu, L. Interrogating single proteins through nanopores: challenges and opportunities. *Trends Biotechnol.* **27**, 333–341 (2009).

26. Zhao, Q., Jayawardhana, D. A., Wang, D. & Guan, X. Study of peptide transport through engineered protein channels. *J. Phys. Chem. B* **113**, 3572–3578 (2009).
27. Oukhaled, G. *et al.* Unfolding of proteins and long transient conformations detected by single nanopore recording. *Phys. Rev. Lett.* **98**, 158101–158104 (2007).
28. Lieberman, K. R. *et al.* Processive replication of single DNA molecules in a nanopore catalyzed by phi29 DNA polymerase. *J. Am. Chem. Soc.* **132**, 17961–17972 (2010).
29. Reiner, J. E., Kasianowicz, J. J., Nablo, B. J. & Robertson, J. W. F. Theory for polymer analysis using nanopore-based single-molecule mass spectrometry. *Proc. Nat. Acad. Sci.* **107**, 12080–12085 (2010).
30. Rotem, D., Jayasinghe, L., Salichou, M. & Bayley, H. Protein detection by nanopores equipped with aptamers. *J. Am. Chem. Soc.* **134**, 2781–2787 (2012).
31. Lu, S., Li, W. W., Rotem, D., Mikhailova, E. & Bayley, H. A primary hydrogen-deuterium isotope effect observed at the single-molecule level. *Nat. Chem.* **2**, 921–928 (2010).
32. Braha, O., Webb, J., Gu, L. Q., Kim, K. & Bayley, H. Carriers versus adapters in stochastic sensing. *ChemPhysChem* **6**, 889–892 (2005).
33. Gu, L. Q., Braha, O., Conlan, S., Cheley, S. & Bayley, H. Stochastic sensing of organic analytes by a pore-forming protein containing a molecular adapter. *Nature* **398**, 686–690 (1999).
34. Astier, Y., Braha, O. & Bayley, H. Toward single molecule DNA sequencing: direct identification of ribonucleoside and deoxyribonucleoside 5′-monophosphates by using an engineered protein nanopore equipped with a molecular adapter. *J. Am. Chem. Soc* **128**, 1705–1710 (2006).
35. Banerjee, A. *et al.* Molecular bases of cyclodextrin adapter interactions with engineered protein nanopores. *Proc. Natl. Acad. Sci. U. S. A.* **107**, 8165–8170 (2010).
36. Koçer, A., Walko, M., Meijberg, W. & Feringa, B. L. A light-actuated nanovalve derived from a channel protein. *Science* **309**, 755–758 (2005).
37. Banghart, M. R., Volgraf, M. & Trauner, D. Engineering light-gated ion channels. *Biochemistry* **45**, 15129–15141 (2006).
38. Loudwig, S. & Bayley, H. Photoisomerization of an Individual Azobenzene Molecule in Water: An On−Off Switch Triggered by Light at a Fixed Wavelength. *J. Am. Chem. Soc.* **128**, 12404–12405 (2006).
39. Misakian, M. & Kasianowicz, J. Electrostatic influence on ion transport through the aHL channel. *J. Membr. Biol.* **195**, 137–146 (2003).
40. Gutsche, C. D. & Alam, I. Calixarenes. 23. The complexation and catalytic properties of water soluble calixarenes. *Tetrahedron* **44**, 4689–4694 (1988).
41. Akeson, M., Branton, D., Kasianowicz, J. J., Brandin, E. & Deamer, D. Microsecond Time-Scale Discrimination Among Polycytidylic Acid, Polyadenylic Acid, and Polyuridylic Acid as Homopolymers or as Segments Within Single RNA Molecules. *Biophys. J.* **3495**, 77153–77155 (1999).
42. Coleman, A. *et al.* Calix[n]arenes as protein sensors. *Creative Chemical Sensor Systems* 31–88 (2007).
43. Gu, L.-Q. & Bayley, H. Interaction of the Noncovalent Molecular Adapter, *β*-Cyclodextrin, with the Staphylococcal α-Hemolysin Pore. *Biophys. J.* **79**, 1967–1975 (2000).
44. McGovern, R. E., Fernandes, H., Khan, A. R., Power, N. P. & Crowley, P. B. Protein camouflage in cytochrome c-calixarene complexes. *Nature Chem.* **4**, 527–533 (2012).
45. Menestrina, G. Ionic channels formed byStaphylococcus aureus alpha-toxin: Voltage-dependent inhibition by divalent and trivalent cations. *J. Membr. Biol.* **90**, 177–190 (1986).
46. Selkti, M. *et al.* The first example of a substrate spanning the calix[4]arene bilayer: the solid state complex of p-sulfonatocalix[4]arene with L-lysine. *Chem. Commun.* 161–162 (2000).
47. Guo, D. S., Wang, L. H. & Liu, Y. Highly effective binding of methyl viologen dication and its radical cation by *p*-sulfonatocalix[4, 5]arenes. *J. Org. Chem.* **72**, 7775–7778 (2007).
48. Wei, Y., Han, S., Kim, J., Soh, S. & Grzybowski, B. A. Photoswitchable catalysis mediated by dynamic aggregation of nanoparticles. *J. Am. Chem. Soc.* **132**, 11018–11020 (2010).
49. Ying, Y. L., Li, D. W., Li, Y., Lee, J. S. & Long, Y. T. Enhanced translocation of poly(dt)45 through an α-hemolysin nanopore by binding with antibody. *Chem. Commun.* **47**, 5690–5692 (2011).
50. Gao, H.-L., Zhang, H., Li, C.-Y. & Xia, X.-H. Confinement effect of protonation/deprotonation of carboxylic group modified in nanochannel. *Electrochim. Acta* (2013) DOI: 10.1016/j.bbr.2011.03.031.

Acknowledgements

This work was supported by the National Base Research 973 Program (2013CB733700). Y.-T.L. is supported by the National Science Fund for Distinguished Young Scholars of China (21125522) and (SKLEAC201305).Y.-L.Y. is supported by the Sino-UK Higher Education Research Partnership for PhD Studies. We thank Mr. Shuaifan Wu for the discussions on synthesis procedures.

Author contributions

Y.-L.Y., J.Z., H.T., I.W. and Y.-T.L. designed research; Y.-L.Y., F.-N.M., C.C. and J.Z. performed research; J.Z. and X.Y. synthesized compounds; Y.-L.Y., F.-N.M. analyzed data; Y.-L.Y., J.Z., Y.-T.L., H.T. and I.W. wrote the paper.

Additional information

Supplementary information accompanies this paper at http://www.nature.com/scientificreports

Competing financial interests: The authors declare no competing financial interests.

How to cite this article: Ying, Y. *et al.* A Stimuli-Responsive Nanopore Based on a Photoresponsive Host-Guest System. *Sci. Rep.* **3**, 1662; DOI:10.1038/srep01662 (2013).